C–H activation

DOI: 10.1002/ange.201305470

Methane Coupling over Magnesium Oxide: How Doping Can Work**

Pierre Schwach, Marc Georg Willinger, Annette Trunschke, and Robert Schlögl*

Dedicated to Professor Helmut Schwarz on the occasion of his 70th birthday

The functionalization of methane remains a challenging target from an academic as well as an industrial point of view.[1] New concepts for the catalytic activation of C–H bonds are needed[1a] to overcome the current limitations in selectivity, which hamper the broad application of methane coupling for the production of olefins from sustainable resources like natural gas and organic waste. Among the various inorganic materials that have been evaluated as heterogeneous catalysts for the oxidative coupling of methane (OCM), alkaline earth oxides doped with alkali elements or transition metal ions have received particular attention.[2] High reaction temperatures (973–1273 K) are needed. However, the high temperature is not required for C–H activation, which may aided by coordinatively unsaturated sites already at low temperature,[3] but rather for recovery of an active catalyst surface free of adsorbed hydroxides and carbonates. Under the harsh reaction conditions, oxide catalysts like Li-MgO undergo fast deactivation due to sintering promoted by water, which is an unavoidable reaction product.[4] Oxygen and magnesium vacancies (V_O'', V_{Mg}'') are involved in the sintering of MgO by facilitating reconstructions due to the enhanced diffusion of lattice ions, which is fast in any case at such high temperatures.[5] On the other hand, vacancies may have an impact on activity and selectivity in catalysis. However, point defects have not detected so far over MgO under realistic working conditions in OCM.

In a recent study, Nilius, Freund, and co-workers et al. provide evidence that strongly bound O_2^- species, precursors of dissociatively adsorbed O_2, are formed on highly ordered CaO films doped with Mo^{2+} ions. The results indicate that molecular activation on doped oxides does not require any surface structural defects.[6] Accordingly, it is suggested that the activation of methane on smooth surfaces of transition-metal-doped wide-band-gap oxides may involve such activated oxygen species.

[*] P. Schwach, Dr. M. Willinger, Dr. A. Trunschke, Prof. Dr. R. Schlögl
Abteilung Anorganische Chemie
Fritz-Haber-Institut der Max-Planck-Gesellschaft
Faradayweg 4–6, 12489 Berlin (Germany)
E-mail: trunschke@fhi-berlin.mpg.de
Homepage: http://www.fhi-berlin.mpg.de/acnew/welcome.epl

[**] We thank M. Hashagen, F. Rybicki, Dr. F. Girgsdies, Dr. M. Eichelbaum, and Dr. O. Timpe for experimental support and scientific discussions. This work was conducted in the framework of the COE "UniCat" (www.unicat.tu-berlin.de) of the German Science Foundation.

Supporting information for this article (including detailed information on catalyst synthesis, characterization, and catalytic tests) is available on the WWW under http://dx.doi.org/10.1002/anie.201305470.

In the present work, we put the concept to test with powder catalysts working at high temperature ($T = 1023$ K). We synthesized doped magnesium oxide as it has been investigated frequently in OCM.[7] Pure magnesium oxide is deactivated at this temperature quite rapidly and reaches a stationary state after a few minutes to several hours depending on the applied contact time and the initial nanostructure of the magnesium oxide. In the stationary state, a low, but constant yield of the coupling products ethane and ethene is obtained over smooth, rounded MgO particles.[8]

We introduced Fe in ppm quantities into MgO. The synthesis of Fe-doped polycrystalline magnesium oxide in which the Fe dopant is homogeneously distributed over the entire bulk is, however, quite challenging and requires highly sensitive analytical techniques for verification. The issue is distributing the dopant throughout the bulk of MgO in such a way that no precipitates or segregated nanostructured dopant phases occur under the drastic reaction conditions. Only then can the validity of the electronic doping concept put forward by Nilius and Freund et al. be tested without interference from other catalytic actions of secondary phases.

The presence of Fe atoms on the surface may introduce additional redox chemistry into the activation mechanism of methane, but, even in an ideal solid solution, terminal Fe atoms cannot be avoided. Therefore, the Fe-MgO catalyst was modified by subsequent adsorption of highly dispersed gold on the surface. An Au-MgO catalyst[9] was included in the study for reference.

The catalysts were synthesized by hydrothermal treatment of MgO in the presence of aqueous solutions of $FeSO_4$, $HAuCl_4$, and a mixture of the two solutions in a microwave autoclave at 483 K and 10 bar for 3 h, followed by annealing in flowing Ar at 1173 K for 3 h. In order to remove potentially segregated transition metal and metal oxide particles, the obtained solids were treated with aqua regia and nitric acid, respectively, and annealed again in Ar at 1123 K for 3 h. X-ray diffraction reveals that the lattice constants of the three doped catalysts do not vary significantly, but the size of the coherently scattering domains (reported from full-pattern X-ray diffraction (XRD) analysis as the volume-weighted mean column length based on integral breadth ($L_{Vol.}IB$)) differs. The largest crystalline domains are found for Au-Fe-MgO, which is also reflected in the lowest specific surface area (Table 1). Structural investigation by transmission electron microscopy (TEM) reveals typical small aggregates consisting of cube-shaped particles that are intergrown and connected mainly along shared faces (Figure 1). The domain size determined by XRD is similar for Fe-MgO and Au-MgO (Table 1) and ranges between 5 and 100 nm according to

Table 1: General characteristics of the doped MgO catalysts and normalized formation rates of coupling products ethane and ethene in OCM of methane.

Catalyst	Fe-MgO	Au-Fe-MgO	Au-MgO
Batch ID[a]	14696	14593	14588
c_{Fe}[b] [ppm]	654	402	–
a[c] [Å]	4.214(1)	4.213(1)	4.214(1)
L_{Vol-IB}[c] [nm]	46(1)	67(1)	47(1)
A[d] [$m^2 g^{-1}$]	32.0	19.9	25.6
r_{C^2}[e] [$\mu mol\, s^{-1} g^{-1}$]	5.12	13.55	0.68
r_{C^2}[e] [$\mu mol\, s^{-1} m^2$]	0.16	0.68	0.03
Redox-active Fe[f]	6%	7%	–

[a] Catalyst ID for clear identification of the batch. [b] Measured by atomic absorption spectroscopy (AAS). [c] Lattice constant of MgO determined by XRD. [d] Specific surface area calculated by applying the BET equation. [e] Formation rate of the coupling products ethane and ethane measured after 4 h time on stream; reaction conditions: $T = 1023$ K, $W/F = 0.033\ g\,s\,mL^{-1}$, $CH_4/O_2/N_2 = 3:1:1$. [f] Percentage of Fe that is accessible at the surface as estimated by temperature-programmed reduction (see Table S1).

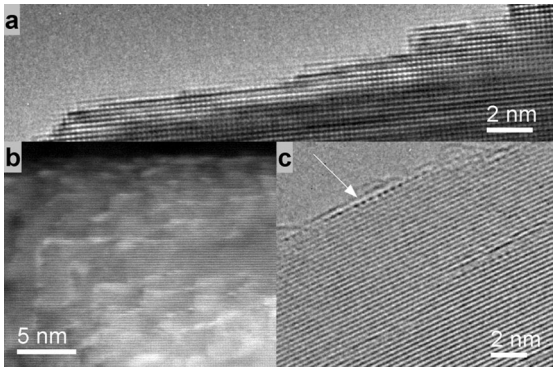

Figure 1. a) HRTEM image showing the stepped surface of Au-Fe-MgO. b) HAADF STEM image with characteristic bright contrast at steps and edges due to decoration with heavy atoms. c) Columns of heavy atoms can also be seen in thin regions in HRTEM.

TEM (Figure 1). The slightly lower specific surface area of Au-MgO indicates that its surface is smoother than that of Fe-MgO.

The UV/Vis spectra of Fe-MgO and Au-Fe-MgO are dominated by an intense absorption in the range of the ligand-to-metal charge-transfer (LMCT) bands (Figure S1). The absorption maximum near 288 nm (34723 cm^{-1}) is attributed to isolated Fe^{3+} ions with octahedral coordination, in other words, on Mg^{2+} lattice positions.[10] EPR spectroscopy confirms the occurrence of Fe^{3+} in cubic symmetry sites in MgO (Figure S2). Contributions of oligomeric species and iron oxide nanoparticles to the UV/Vis spectra cannot be excluded due to the complex fine structure and the extended tail of the bands towards decreasing energy. However, no aggregates of iron were detected by TEM, indicating high Fe dispersion. Since the Fe concentration is low, the weak absorption due to d–d transitions in the range between 330 nm (30000 cm^{-1}) and 1000 nm (10000 cm^{-1}) gives featureless, very weak, and broad bands that do not allow unambiguous interpretation with respect to the coordination environment of Fe^{3+} (d^5) ions, and potentially appearing Fe^{2+} (d^6) ions. The spectra of the gold-containing catalysts exhibit the characteristic surface plasmon mode around 520 nm (19230 cm^{-1}) that is ascribed to gold nanoparticles.[11] The broad appearance of the band suggests that Au occurs in different particle sizes ranging from atomic dimensions to Au particles with a diameter of about 10 nm.[12] Indeed, very rare and scarcely distributed isotropic gold nanoparticles can be found on the surface of the MgO particles by TEM.

Temperature-programmed reduction (TPR) and oxidation (TPO) cycles were performed to analyze the redox properties of the Fe-containing MgO catalysts (Figures S3 and S4). In the first run, the catalysts were heated in inert gas and evolution of hydrogen was observed in a temperature range between 573 and 673 K and under isothermal conditions at 1073 K; the results indicated the formation of point defects in the bulk of Fe-MgO and Au-Fe-MgO during the thermal pretreatment.[13] The hydrogen-consumption profile of the first TPR run differs from that of the second and third runs, which were performed in each case after intermediate temperature-programmed oxidation. In contrast, the second and third TPR profiles are identical, indicating the high reversibility, stability, and absence of segregation processes after initial stabilization during the first cycle. This applies to Fe-MgO (Figure S3) as well as to Au-Fe-MgO (Figure S4), indicating that the catalysts are comparable, in particular, because the bulk oxide properties, which were sensed by redox probing, are quite similar and in agreement with the XRD results. The first TPR run reveals a dopant-induced difference between the two catalysts. In addition to the two high-temperature peaks around 810–840 K and 1050–1060 K, Fe-MgO exhibits an additional hydrogen-consumption peak at low temperature (513 K) arising from easily reducible Fe species. The peak does not appear again in subsequent cycles indicating the dissolution of the species into the bulk where it is protected from reoxidation. The amount of consumed hydrogen proves that only a minor fraction of the low-level iron doping is susceptible to reduction on the surface (Table 1 and Table S1); this indicates the homogeneous distribution of the dopant within the bulk of magnesium oxide. The fraction of reducible iron is initially higher in Fe-MgO than in Au-Fe-MgO, indicating that surface iron species are shielded by topping gold species.

The low yield of coupling products in OCM as presented in Figure 2 was deliberately measured at short contact times to prevent full oxygen conversion and thus to allow a meaningful kinetic comparison. Gold seems to block the active sites on the surface of MgO since Au-MgO shows only negligible activity. This is ascribed to the propensity of gold to adsorb at step edges of the MgO surface and thus cover the active sites related to edges.[14] Fe-MgO is more active (Figures S5 and S6) and selective (Figure S7) resulting in higher yield. The behavior of Fe-MgO at the beginning of the experiment is attributed to the presence of surface redox-active iron species, in accordance with the observations made by TPR. Further increase in methane conversion and selectivity is achieved by codoping with Fe and Au. The synergistic effect of the two transition metal additives becomes even more apparent by

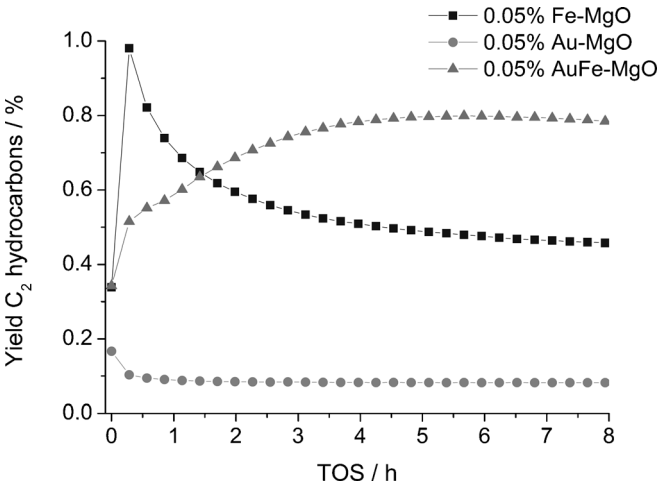

Figure 2. Yield of ethane and ethene in the oxidative coupling of methane as a function of time on stream (TOS) at $T = 1023$ K; $W/F = 0.0167$ g s mL^{-1}; $CH_4/O_2/N_2 = 3:1:1$.

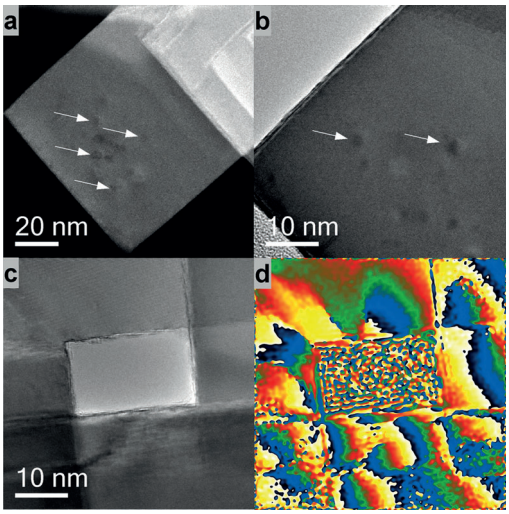

Figure 3. a) HAADF STEM and b) TEM image with localized contrast variations due to defects caused by bulk doping as indicated by arrows. c) HRTEM image of doped MgO particles; the lattice rotation due to strain is shown in (d).

comparison of the rate of C_2 formation normalized to the specific surface area of the catalyst (Table 1). After a formation period with increasing activity, Au-Fe-MgO shows stable activity at the time scale of the present experiment. This behavior is surprising and novel for alkaline earth metal oxide based catalysts.

An explanation may be provided by electron microscopy. High-angle angular dark-field scanning transmission electron microscopy (HAADF STEM), which is sensitive to variations in atomic weight can be used to locate the heavier dopant atoms in the MgO matrix. As can be seen in Figure 1, corners and edges are characterized by brighter contrast, indicating the presence of either Au or Fe. This is confirmed by HRTEM images recorded from thin regions of MgO crystals, where rows of strongly scattering atoms are detected at surface steps even after catalytic testing (Figure 1c and Figure S8). These atoms will suppress the action of steps as active sites and thus poison the Au-MgO catalyst, which does not have sites caused by electronic doping. In addition, investigation of the bulk structure by HAADF STEM and TEM reveals the presence of local strain, causing particular contrast variations such as indicated in Figure 3a,b. Analysis of the lattice fringes[15] shows doping-induced strain and lattice rotation, as visualized in Figure 3c,d. Due to the low concentration, energy-dispersive X-ray (EDX) elemental analysis is not sensitive enough to clarify whether the defects are caused by gold or iron incorporation into the MgO lattice.

The sintering behavior of Au-Fe-MgO is similar to that of undoped MgO. Initially, the surface of the cube-shaped particles exposes stepped and atomically flat planes (Figure 1). Steps are usually in the range of half (one atom) and single unit cell height (Figure 1a). During the catalytic reaction, the abundance of such small steps decreases and larger steps form. Despite these sintering phenomena, the catalytic activity of the Au-Fe-MgO catalyst shows appreciable stability. This is a clear indication that the lasting activity is not due to the conversion of methane at steps but rather at sites located at terraces. Doping has changed the nature of the active sites as indicated clearly by the temporal evolution of the catalytic activity shown in Figure 2 and Figures S5–S7. The inverse trend for the codoped system as compared to the other systems points to the formation of active sites for oxygen activation in Au-Fe-MgO during time on stream, whereas the other systems are deactivated through the loss of monatomic step sites following surface transformation caused by the reaction products water and CO_2. The stable minimal activity of the Au-MgO system marks the intrinsic activity of active sites in the present MgO catalyst that are not associated with step edges. Compared to this activity (see Table 1) the electronic doping by Fe increases the rate of C_2 formation by over an order of magnitude.

For the classical Au-MgO system it was found that small doping levels produce metallic and some chemically active gold species, which decorate steps and thus reduce the activity of the parent MgO exactly as found in the present study.[9] Only at much higher doping levels were catalytic effects described and associated with Au particles and defect formation in MgO. In the present study two types of gold were evidenced based on the catalytic results: In single doped Au-MgO only the step-decorating poisoning effect was found. Through the presence of subsurface iron species in the codoped system the edge-decorating effect was massively overruled by the beneficial effect of creating structurally stable novel active sites at terraces of the MgO without introducing vacancies that may destabilize the system at longer time on stream. This second gold species apparently arises from a significant gold–support interaction stemming from the strain in the MgO due to iron doping. The possible effects of isotropic unstrained gold particles are negligible in the present study due to their very low abundance as a consequence of the synthesis strategy. Electronic doping of MgO terraces is also achieved through iron dissolution only, but with significant lower effectiveness. It is tempting to conclude that the codoping creates highly active sites for

oxygen activation to give a peroxy species,[16] whereas iron doping ends up with sites creating oxo species that are less active in creating methyl radicals for OCM.

The purpose of the present work was to elucidate, much along the demand of Hutchings,[17] how electronic promoters may change the reaction pathway of the OCM reaction. Stimulated through the clear-cut model observation of Nilius, Freund et al. we synthesized a polycrystalline form of a model compound exhibiting the same subsurface doping as evidently achieved in the their model system. By carefully avoiding the formation of nanoparticles of the transition metal oxide we observed the predicted doping effect without interference from total oxidation of the methane molecule.

It was not our intention to explore the potential of this electronic effect with respect to selectivity and yield. We rather wanted to demonstrate by a catalytic experiment that an electronic doping effect predicted by chemical physics exists for alkali earth oxides and affects oxygen activation. An additional benefit is the amplification of this doping effect by gold as a result of its specific interaction with MgO at iron-modified sites. As the doping procedure is reproducible and the levels of doping species are low, it is conceivable that the concept of homogeneous electronic doping of alkali earth oxides may find application for the stabilization of realistic systems.

Received: June 25, 2013
Published online: September 17, 2013

Keywords: alkaline earth oxides · defects · doping · heterogeneous catalysis · oxidative coupling

[1] a) H. Schwarz, *Angew. Chem.* **2011**, *123*, 10276; *Angew. Chem. Int. Ed.* **2011**, *50*, 10096; b) C. Hammond, S. Conrad, I. Hermans, *ChemSusChem* **2012**, *5*, 1668.
[2] U. Zavyalova, M. Holena, R. Schlögl, M. Baerns, *ChemCatChem* **2011**, *3*, 1935.
[3] T. Ito, T. Watanabe, T. Tashiro, K. Toi, *J. Chem. Soc. Faraday Trans. 1* **1989**, *85*, 2381.
[4] a) U. Zavyalova, M. Geske, R. Horn, G. Weinberg, W. Frandsen, M. Schuster, R. Schlögl, *ChemCatChem* **2011**, *3*, 949 – 959; b) U. Zavyalova, G. Weinberg, W. Frandsen, F. Girgsdies, T. Risse, K. P. Dinse, R. Schloegl, R. Horn, *ChemCatChem* **2011**, *3*, 1779 – 1788.
[5] D. Beruto, A. W. Searcy, R. Botter, M. Giordani, *J. Phys. Chem.* **1993**, *97*, 9201 – 9205.
[6] Y. Cui, N. Nilius, X. Shao, M. Baldofski, J. Sauer, H.-J. Freund, *Angew. Chem.* **2013**, DOI: 10.1002/ange.201305119; *Angew. Chem. Int. Ed.* **2013**, DOI: 10.1002/anie.201305119.
[7] J. H. Lunsford, *Angew. Chem.* **1995**, *107*, 1059 – 1070; *Angew. Chem. Int. Ed. Engl.* **1995**, *34*, 970 – 980.
[8] J. S. J. Hargreaves, G. J. Hutchings, R. W. Joyner, C. J. Kiely, *J. Catal.* **1992**, *135*, 576 – 595.
[9] K. Blick, T. D. Mitrelias, J. S. J. Hargreaves, G. J. Hutchings, R. W. Joyner, C. J. Kiely, F. E. Wagner, *Catal. Lett.* **1998**, *50*, 211 – 218.
[10] G. Lehmann, *Z. Phys. Chem. Neue Folge* **1970**, *72*, 279 – 297.
[11] C. F. Bohren, D. R. Huffman, *Absorption and Scattering of Light by Small Particles*, Wiley, New York, **1983**.
[12] K. C. Grabar, R. G. Freeman, M. B. Hommer, M. J. Natan, *Anal. Chem.* **1995**, *67*, 735 – 743.
[13] B. V. King, F. Freund, *Phys. Rev. B* **1984**, *29*, 5814 – 5824.
[14] J. S. J. Hargreaves, G. J. Hutchings, R. W. Joyner, C. J. Kiely, *Catal. Today* **1992**, *13*, 401 – 407.
[15] M. J. Hÿtch, E. Snoeck, R. Kilaas, *Ultramicroscopy* **1998**, *74*, 131.
[16] P. Landon, P. J. Collier, A. J. Papworth, C. J. Kiely, G. J. Hutchings, *Chem. Commun.* **2002**, *0*, 2058.
[17] G. J. Hutchings, *Catal. Lett.* **2001**, *75*, 1.

